

RESEARCH

Open Access



Computational study on the mechanism of small molecules inhibiting NLRP3 with ensemble docking and molecular dynamic simulations

Pingyang Qin¹, Yuzhen Niu^{1*}, Jizheng Duan² and Ping Lin^{1*}

Abstract

NLRP3 (Nucleotide-binding oligomerization domain, LRR and pyrin domain-containing protein 3) is a pivotal regulator of inflammation, with strong implications in gout, neurodegenerative diseases, and various inflammatory conditions. Consequently, the exploration of NLRP3 inhibitors is of great significance for the treatment of diseases. MCC950, NP3-146, compound (3), and YQ128 are four highly bioactive NLRP3 inhibitors that show great potential; however, their mechanism of action is currently limited to targeting the ATP binding region (NACHT site) of the NLRP3 protein. To gain deeper insights into the defining features of NLRP3 inhibitors and to develop more potent inhibitors, it is imperative to elucidate the interaction mechanism between NLRP3 and these inhibitors. In this study, we employ a comprehensive computational approach to investigate the binding mechanism between NLRP3 and representative inhibitors. Utilizing the molecular mechanics/generalized Born surface area (MM/GBSA) method, we calculate the binding free energy and pinpoint the key residues involved in the binding of the four inhibitors to NLRP3. The decomposition of binding free energy by the MM/GBSA method reveals that the residues Val71, Arg195, Ile255, Phe419, Arg422, and Met505, situated around the binding pocket, play a crucial role in conferring the high bioactivity of NLRP3 inhibitors. Furthermore, pharmacophore analysis of the four NLRP3 complexes indicates that the primary interaction between the inhibitors and NLRP3 was mainly hydrophobic interaction. Our study provides a profound understanding of the interaction mechanism between NLRP3 and its inhibitors, identifies the key residues involved, and provides theoretical guidance for the design of more efficient NLRP3 inhibitors.

Keywords NLRP3, Promising NLRP3 inhibitors, Comprehensive calculation strategy, Ensemble docking, Binding free energy calculations

*Correspondence:

Yuzhen Niu
niuyzh12@lzu.edu.cn
Ping Lin
linping@wfust.edu.cn

¹College of Chemical Engineering and Environment, Weifang University of Science and Technology, Weifang 262700, China

²Institute of Modern Physics, Chinese Academy of Science, Lanzhou 730000, China



© The Author(s) 2025. **Open Access** This article is licensed under a Creative Commons Attribution-NonCommercial-NoDerivatives 4.0 International License, which permits any non-commercial use, sharing, distribution and reproduction in any medium or format, as long as you give appropriate credit to the original author(s) and the source, provide a link to the Creative Commons licence, and indicate if you modified the licensed material. You do not have permission under this licence to share adapted material derived from this article or parts of it. The images or other third party material in this article are included in the article's Creative Commons licence, unless indicated otherwise in a credit line to the material. If material is not included in the article's Creative Commons licence and your intended use is not permitted by statutory regulation or exceeds the permitted use, you will need to obtain permission directly from the copyright holder. To view a copy of this licence, visit <http://creativecommons.org/licenses/by-nc-nd/4.0/>.

Introduction

Inflammation is a common physiological and pathological process in the body, and the inflammatory corpuscles play an crucial regulatory role in inflammatory response [1]. To date, five types of inflammasomes have been identified: NLRP1, NLRP3, NLR family, CARD domain containing 4(NLRC4), Interstitial Pneumonia with Autoimmune Features(IPAF) and Absent In Melanoma 2(AIM2) [2]. Among these, NLRP3 is a key regulatory protein that participates in the formation of the NLRP3 inflammasome complex [3]. It has been observed that the activation of NLRP3 and its associated molecular regulatory signal pathways are closely associated with the onset and progression of various diseases, including nonalcoholic steatohepatitis (NASH), gout, porphyria-associated periodic syndrome, inflammatory bowel disease, and neurodegenerative diseases. These findings have garnered widespread attention and represent a frontier and hot area of clinical drug research and development [4, 5]. The NLRP3 sensor protein comprises three domains: The N-terminal pyrin domain (PYD), the nucleotide binding oligomerization domain (NACHT) with ATP catalytic function, and the C-terminal leucine-rich repeat (LRR) [6]. Under normal conditions, NLRP3 expression is low, and it is maintained in a self-inhibition state by the LRR region (Fig. 1). Upon recognition of pathogen-associated molecular patterns (PAMPs) or danger-associated molecular patterns (DAMPs) by the host, nuclear factor- κ B (NF- κ B) can be activated, initiating the transcription of NLRP3. The activated PYD of NLRP3 binds to the PYD domain of ASC (apoptosis-associated

speck-like protein containing a CARD), leading to the formation of ASC specks through oligomerization. Subsequently, the CARD domain of ASC interacts with the CARD domain of pro-caspase-1. This oligomeric form of pro-caspase-1 undergoes self-cleavage to produce caspase-1, which then catalytically processes pro-IL-1 β and pro-IL-18 into their active forms, ultimately triggering inflammation [7].

At present, numerous NLRP3 small molecule inhibitors have been reported, with MCC950 being a notable example [8], MCC950 efficiently and selectively inhibits NLRP3, with an IC₅₀ of inhibiting IL-1 β at the cellular level of 7.5nM [9]. It has also been shown to reduce mortality in newborn mice in a cryopyrin-associated periodic syndrome (CAPS) mouse model, demonstrating the compound's efficacy [10]. Other NLRP3 inhibitors with good activity include NP3-146 [11], compound(3) [12] and YQ128 [13] are all NLRP3 inhibitors with well activity. They also exhibit significant differences in biological activity. Dekker et al. [11] reported the crystal structure of NP3-146 and NLRP3 complex for the first time, providing valuable insights into the molecular-level interaction mechanism between NLRP3 and its inhibitors. Prior to this structural insight, researchers had shown that these inhibitors primarily target the ATP-binding region of the NLRP3 protein (i.e., the NACHT domain), thereby inhibiting its ATP hydrolysis activity and subsequently preventing the oligomerization and assembly of the inflammasome complex. Therefore, studying the interaction mechanism between NLRP3 and its representative inhibitors is of great importance for understanding

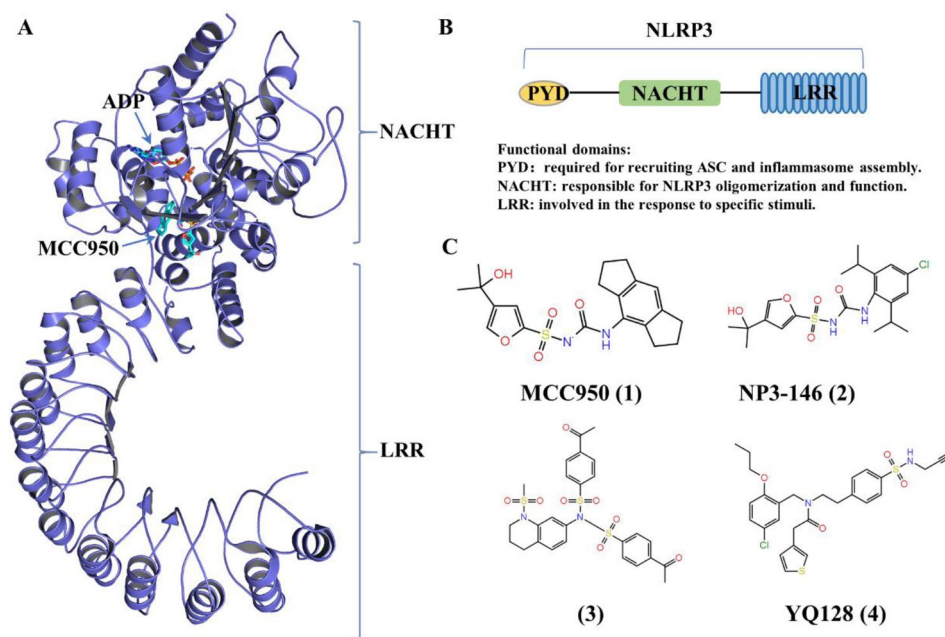


Fig. 1 **A** The structure of NLRP3, the inhibitor binds to the region of NACHT, purple cartoon represents NLRP3, blue sticks represent ligands MCC950 and ADP; **B** The functional area division of NLRP3; **C** The inhibitors studied in this work

the key features of NLRP3 inhibitors and for the development of more effective NLRP3 inhibitors.

Molecular dynamics (MD) simulation and binding free energy calculation tools are widely utilized in drug design [14–19], providing valuable insights into the dynamic structure of protein-ligand interactions [20–24]. Based on MD trajectories, numerous methods have been developed to predict binding free energy, including free energy perturbation (FEP) [25], thermodynamic integration (TI) [26] and molecular mechanics/generalized Born surface area (MM/GBSA) method [27]. Compared to FEP or TI, MM/GBSA method offers a favorable balance between computational speed and accuracy, making it a popular choice for various protein-ligand systems, such as kinase systems, viral proteins, and other functional proteins [28–31].

Therefore, in this study, a comprehensive computational strategy was employed to elucidate the binding mode of NLRP3 and its representative inhibitors. Initially, the structures of the complexes formed by the four NLRP3 inhibitors— MCC950, NP3-146, compound (3) and YQ128 (Fig. 1) — with NLRP3 were obtained through molecular docking methods of varying precision. Subsequently, these four systems were subjected to conventional molecular dynamics simulations for 1 microsecond. Finally, by analyzing the trajectories from these simulations in conjunction with free energy calculations and energy decomposition, key residues that play crucial roles in the binding of inhibitors to NLRP3 were identified. Currently, there is limited research on NLRP3 computational studies; thus, gaining direct insights into the key interactions between NLRP3 and its inhibitors at the protein level will significantly advance the development of NLRP3 inhibitors.

Materials and methods

Ensemble docking

The docking of NLRP3 and ligands was performed using Schrodinger 2015. The crystal structure of the NLRP3 complex of the drug NP3-146, which is the focus of our study, has been determined. Therefore, we retrieved the initial structure of the NLRP3/NP3-146 complex from the RCSB Protein Data Bank (PDB ID code:7ALV [11]). Missing residues were added and aligned using Schrodinger 2015. Subsequently, the structure of the NLRP3/NP3-146 complex was prepared using the *Protein Preparation Wizard*, which involved adding side chains to residues, assigning protonation states, hydrogen atoms, and relaxing the side chains of the proteins.

To obtain a more accurate initial pose, induced Fit Docking (IFD) was performed in Schrodinger 2015 [32]. The protein molecule was minimized with an RMSD cut-off of 0.20 Å, and the centroid of the residues was automatically generated. The initial docking for each ligand was carried out using Glide. Residues within 5.0 Å of the ligand position were carefully selected for the side chain optimization, ensuring that the structure and conformation adapted to each pose of the protein. The ligand was rigorously docked into the protein structure suitable for induction, and as a result, an IFD score was generated for each output pose.

Systems setup and molecular dynamics (MD) simulations

The partial charges of the four ligands were calculated at the HF/6-31G(d) level of theory and then fixed using the RESP methodology [33–35]. Each receptor-ligand complex was subsequently parameterized using the AMBER14SB [36] and GAFF force fields. The complexes were solvated with the TIP3P water model [37] in a 10 Å cubic box using Leap, and Cl⁻ ions were added to neutralize the net +2 charge of the system (the salt concentration is about 2.5×10^{-3} M).

All of the MD simulations were performed using the AMBER20 package. Initially, a steepest-descent minimization scheme was applied to the systems for 40,000 steps. The systems were then gradually heated from 0 to 310 K over 100 ps in the NVT ensemble, with weak harmonic restraints of a constant force of 10 kcal/mol·Å² applied to the C and N atoms of the protein backbone. Subsequently, the restraints were gradually decreased over 0.9 ns from 10 to 0.01 kcal/mol·Å². Finally, 1 μs MD simulations were conducted at a temperature of 310 K and a pressure of 1 atm without any restraints. Throughout the simulation process, short-range non-bonded interactions were computed using a cutoff distance of 10 Å, while long-range electrostatic interactions were treated using the Particle Mesh Ewald (PME) algorithm [38]. The SHAKE algorithm [39] was used to constrain all bonds involving hydrogen atoms, and the time step was set to 2 fs.

Thermodynamic calculation

The Molecular Mechanics/Generalized Born Surface Area (MM/GBSA) approach [40, 41], commonly used to elucidate receptor-ligand interaction mechanisms, was employed to estimate the binding free energies for the protein-ligand complex [23, 42–48]. Within the MM/GBSA framework, the binding free energy is decomposed

into several components. For the free energy calculations, 500 snapshots were extracted from the final 200ns of the MD trajectory for free energy calculations. These calculations were performed in AMBER20, and the binding free energy can be computed as follows:

$$\langle \Delta G_{bind} \rangle = \langle \Delta E_{MM} \rangle + \langle \Delta G_{solvation} \rangle - T \langle \Delta S_{MM} \rangle \quad (1)$$

Where $\langle \Delta G_{bind} \rangle$ refers to the calculated average free energy, and $\langle \Delta E_{MM} \rangle$ refers to the average molecular mechanical energy.

$$\langle \Delta E_{MM} \rangle = \langle \Delta E_{bond} \rangle + \langle \Delta E_{angle} \rangle + \langle \Delta E_{tors} \rangle + \langle \Delta E_{vdw} \rangle + \langle \Delta E_{elec} \rangle \quad (2)$$

$$\langle \Delta G_{solvation} \rangle = \langle \Delta G_{GB} \rangle + \langle \Delta G_{SA} \rangle \quad (3)$$

$\langle \Delta G_{solvation} \rangle$ refers to the desolvation free energy upon ligand binding. The polar contribution of desolvation ($\langle \Delta G_{GB} \rangle$) was calculated based on the Generalized Born (GB) model, with the *igb* parameter set to 2. The dielectric constants for solute and solvent were set to 1 and 80, respectively. The nonpolar contribution of desolvation ($\langle \Delta G_{SA} \rangle$) was determined by the solvent accessible surface area (SASA) using the LCPO method [49], with the formula $\Delta G_{SA} = 0.0072 \times \Delta SASA$. The normal-mode analysis [50] was utilized to estimate the conformational entropy contribution ($-T \langle \Delta S \rangle$) upon ligand binding, using 500 snapshots extracted from the MM/GBSA calculations.

Construction of pharmacophore modeling

AncPhore [51] is utilized to identify the key pharmacophore features of the interactions between receptors and ligands in the four systems. As a plug-in of PYMOL, AncPhore is implemented in C/C++, and automatically recognizes the essential pharmacophore characteristics for the receptor-ligand complex. The pharmacophore model structure is derived from the average structure of the last 200ns of equilibrium trajectory extracted from the MD simulation. The key pharmacophore features are then established and imported into PYMOL for visualization and mapping.

Results and discussion

Initial poses of inhibitors binding to NLRP3

As shown in Fig. S1, we obtained the bound modes of four inhibitors—MCC950(A), NP3-146(B), (3)(C) and YQ-128(D)—with NLRP3 using molecular docking

techniques. MCC950 and NP3-146 share structural similarities, which manifest in their comparable binding interactions with NLRP3. Specifically, both inhibitors establish hydrophobic contacts with a series of the residues including Ala71, Gly73, Arg195, Pro196, Val197, Phe254, ILE255, Thr283, Tyr287, Thr368, Ile418, Arg422, Phe423, Gln468 and Glu473. Additionally, they form hydrogen bond with Gly73 and Arg422.

However, subtle conformational differences between MCC950 and NP3-146 result in a distinct hydrogen bonding mode; MCC950 forms an extra hydrogen bond with Gln468 that is absent in NP3-146. In contrast, the binding mode of compound (3) with NLRP3 differs significantly from that of MCC950, despite remaining within the confines of the preset binding pocket. As depicted in Fig. S1, compound (3) exclusively forms a hydrogen bond with the residue Arg422, highlighting a shift in the key interaction points compared to MCC950 and NP3-146. The binding mode of YQ-128 with NLRP3 exhibits some similarities to that of compound (3), yet it also displays unique features. YQ-128 establishes hydrogen bonds with residues Ile214, Tyr476, and Asp506, indicating a distinct interaction profile compared to the other inhibitors. These preliminary differences in binding modes were identified through molecular docking, providing a snapshot of the potential interactions between the inhibitors and NLRP3. To delve deeper into these interactions and uncover more nuanced differences, we plan to conduct comprehensive molecular dynamics simulations on these four complex systems. This approach will allow us to gain a more detailed understanding of the dynamic nature of the inhibitor-NLRP3 interactions and potentially reveal new insights into the mechanism of action of these inhibitors.

Stability of MD simulations

The accuracy and reliability of the docking poses of four inhibitors with NLRP3 were assessed through all-atom explicit solvent MD simulations, and a total of 1 μ s of simulation trajectories was collected for analysis. To assess the stability of the four complexes, we monitored the root-mean-square deviation (RMSD) values computed on the backbone atoms of the protein and the heavy atoms of the ligand throughout the simulation process. As illustrated in Fig. S2, after approximately 500 ns of simulation, both the heavy atoms of the inhibitor and the residues within 5 Å of the binding pocket exhibited relatively small conformational changes, with RMSD values remaining below 1 Å. This indicated that each complex had reached a stable equilibrium state. However, it is

worth noting that the residues within 5 Å of the ligand compound (3) and the heavy atoms of compound (3) displayed greater fluctuations compared to the other complexes. This is attributed to the inherent flexibility of compound (3). Despite these fluctuations, the RMSD values remained within a range of ± 1 Å, suggesting that the system had still achieved a dynamic equilibrium. Therefore, we can conclude that the docking poses of all four inhibitors with NLRP3 are reliable and stable under the conditions of our MD simulations.

Binding free energies calculations

The binding free energy of the four complexes was calculated using the MM/GBSA method to investigate the distinct mechanisms by which these inhibitors interact to NLRP3 and to quantify the contributions of various components to the binding free energy (ΔG_{bind}). The contributions of ΔG_{bind} are summarized in Table 1.

As evident from Table 1, both van der Waals interactions (ΔE_{vdw}) and electrostatic interactions (ΔE_{ele}) play crucial roles in facilitating the binding of the inhibitors to NLRP3. The van der Waals interactions contribute negatively to the binding free energy for all inhibitors, indicating their favorable energetic contribution to binding. Similarly, the electrostatic interactions also contribute negatively for MCC950 and NP3-146, but less so for (3) and YQ128, suggesting a relatively weaker electrostatic attraction in these latter two complexes. Notably, there is no significant variation in the calculated nonpolar component of the binding free energy ($\Delta G_{\text{nonpolar}} = \Delta E_{\text{vdw}} + \Delta G_{\text{SA}}$) across the complexes. This suggests that the nonpolar interactions, which are primarily driven by van der Waals forces and surface area burial, contribute similarly to the binding affinity of all inhibitors. However, marked differences are observed in the

polar component ($\Delta G_{\text{polar}} = \Delta E_{\text{ele}} + \Delta G_{\text{GB}}$), primarily stemming from differences in ΔE_{ele} and the polar solvation energy (ΔG_{GB}). The polar component contributes positively to the binding free energy for all inhibitors, but the magnitude of this contribution varies significantly. For MCC950, the polar component is relatively small and negative, indicating a favorable electrostatic interaction that stabilizes the complex. In contrast, for the other inhibitors, the polar component is larger and positive, suggesting a less favorable electrostatic interaction. These disparities result in substantial variations in the final binding free energy values. Specifically, the ΔG_{bind} for the NLRP3/MCC950 complex is markedly lower than that for the other three complexes. This finding indicates that MCC950 exhibits significantly higher binding affinity for NLRP3 compared to the other inhibitors, which aligns well with the experimental data on inhibitory activity. As the most potent NLRP3 inhibitor among those studied, MCC950's binding to NLRP3 is characterized by a notable difference in the electrostatic component. The favorable electrostatic interaction in the MCC950 complex is likely due to a combination of favorable charge-charge interactions and a favorable polar solvation energy. Additionally, the van der Waals contribution to the binding free energy also constitutes a significant portion for MCC950, further stabilizing the complex.

On the other hand, the entropy contribution ($-T\Delta S$) remains relatively unchanged across the inhibitors. This suggests that the changes in binding affinity are primarily driven by changes in the enthalpic components of the binding free energy, rather than by changes in the entropy of binding. In the subsequent analysis, we will delve into the reasons behind these differences by examining the energy decomposition and binding modes of all inhibitors with NLRP3. This will provide further insights into the distinct mechanisms by which these inhibitors interact with NLRP3 and how their binding affinities are modulated by various energetic contributions.

Table 1 Binding free energy predicted by MM/GBSA method

Contribution	MCC950	NP3-146	(3)	YQ128
ΔE_{ele}	-54.05 ± 0.52	-27.52 ± 0.27	-37.41 ± 0.27	-19.82 ± 0.21
ΔE_{vdw}	-45.24 ± 0.13	-46.62 ± 0.14	-51.69 ± 0.15	-43.43 ± 0.16
ΔG_{SA}	-6.14 ± 0.01	-6.96 ± 0.01	-6.37 ± 0.01	-7.89 ± 0.02
ΔG_{GB}	54.97 ± 0.42	39.51 ± 0.18	58.79 ± 0.25	37.89 ± 0.18
$\Delta G_{\text{nonpolar}}^a$	-51.38 ± 1.12	-53.58 ± 1.45	-58.06 ± 2.56	-51.32 ± 2.81
$\Delta G_{\text{polar}}^b$	0.92 ± 2.14	11.99 ± 3.45	21.38 ± 3.24	18.07 ± 0.48
ΔG_{Total}	-50.46 ± 0.20	-41.59 ± 0.13	-36.68 ± 0.17	-33.25 ± 0.14
$-T\Delta S$	23.24 ± 4.78	26.53 ± 4.56	25.63 ± 5.21	23.83 ± 4.89
ΔG_{Bind}	-27.22 ± 6.24	-15.06 ± 4.67	-11.05 ± 6.98	-9.42 ± 8.59
$IC_{50}(\text{nM})$	7.5	80	274	300

$$^a \Delta G_{\text{nonpolar}} = \Delta E_{\text{vdw}} + \Delta G_{\text{SA}}$$

$$^b \Delta G_{\text{polar}} = \Delta E_{\text{ele}} + \Delta G_{\text{GB}}$$

Binding mechanism of inhibitors in the NLRP3

To conduct a more precise assessment of the distinct binding modes of the four inhibitors with NLRP3, we derived the average structure from the MD equilibrium trajectory and tracked the hydrogen bond occupancy between the receptor and ligand throughout this trajectory. As illustrated in Figs. 2 and 3 and a consistent binding feature of the inhibitors observed for all inhibitors with NLRP3, when compared to the initial structure, is the stable persistence of a hydrogen bond between residue 422 and the inhibitor throughout the entire MD

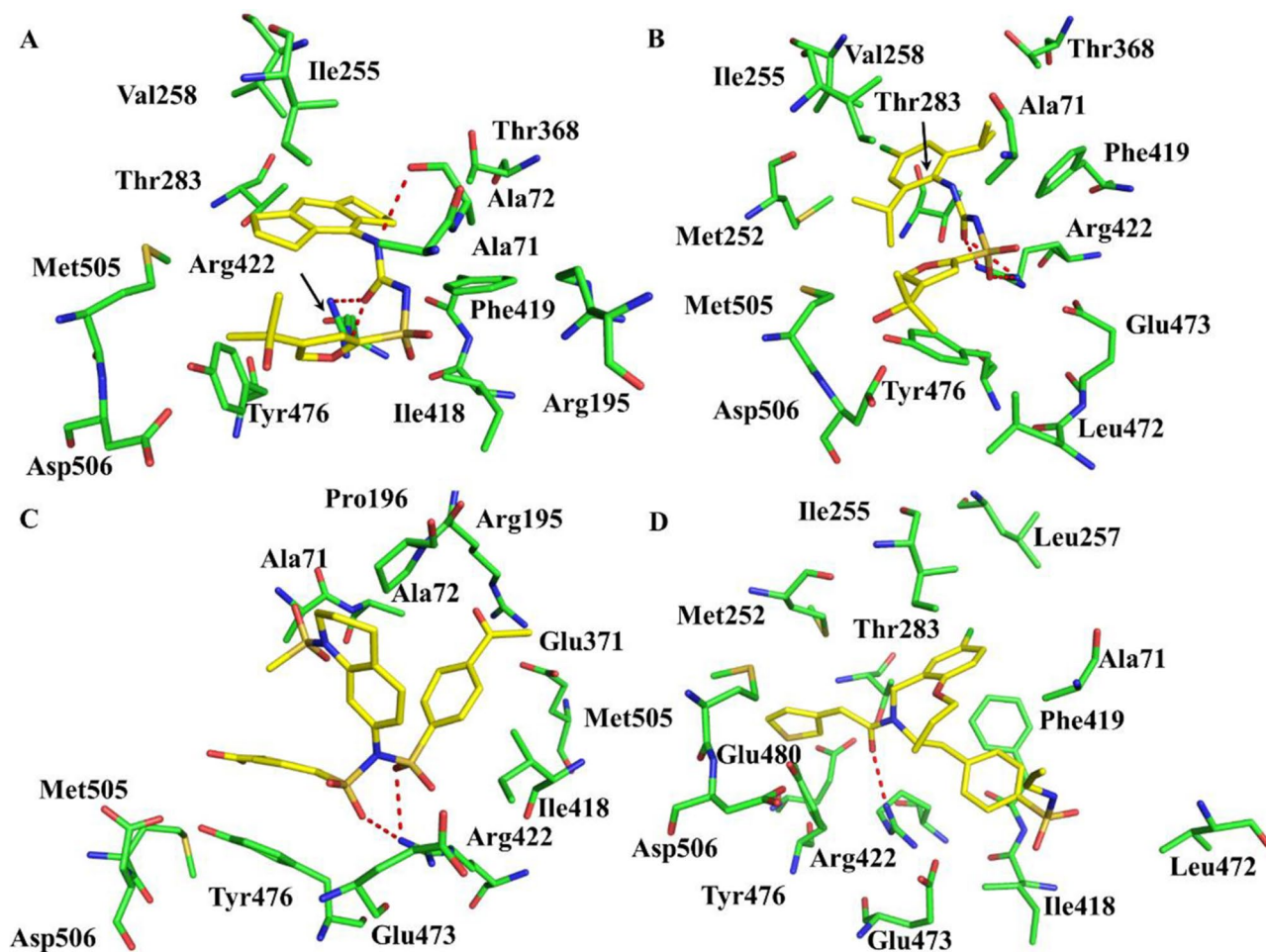


Fig. 2 The binding mode of the stable conformations of the four complex systems obtained from the equilibrium trajectories of MD simulations, the green sticks represent key residues in the pocket of NLRP3 and the yellow sticks represent ligands. (A) NLRP3/MCC950 complex; (B) NLRP3/NP3-146 complex; (C) NLRP3/(3) complex; (D) NLRP3/YQ128 complex

simulation (Table 2), which aligns with the initial binding conformations. Specifically, in the MCC950/NLRP3 complex, hydrogen bonds between residue Ala72 and MCC950 exhibit occupancy rates of approximately 39% and 25%, depending on whether Ala72 acts as the acceptor or donor, respectively. Additionally, several hydrogen bonds with lower occupancy rates were detected between residue Asp506 and MCC950 (~34% and 29%). In the NP3-146/NLRP3 complex, stable hydrogen bonds formed by residues Arg422 and Asp506 with NP3-146 were also observed. These findings underscore the significance of hydrogen bonds in enhancing the stability of the interaction between inhibitors and the target protein.

In the complex involving compound (3) and NLRP3, hydrogen bonds are formed between residues Arg422 and Val197 with compound (3); however, only the hydrogen bond contribution from residue Arg422 was noted in the YQ128/NLRP3 complex. These observations corroborate the numerical differences in the predicted binding free energies between NLRP3 and the four inhibitors.

Per-residue energy contribution analysis of inhibitors binding to NLRP3

We employed the MMPBSA method to calculate the enthalpy change component of the binding free energy between the four inhibitors and NLRP3, and further

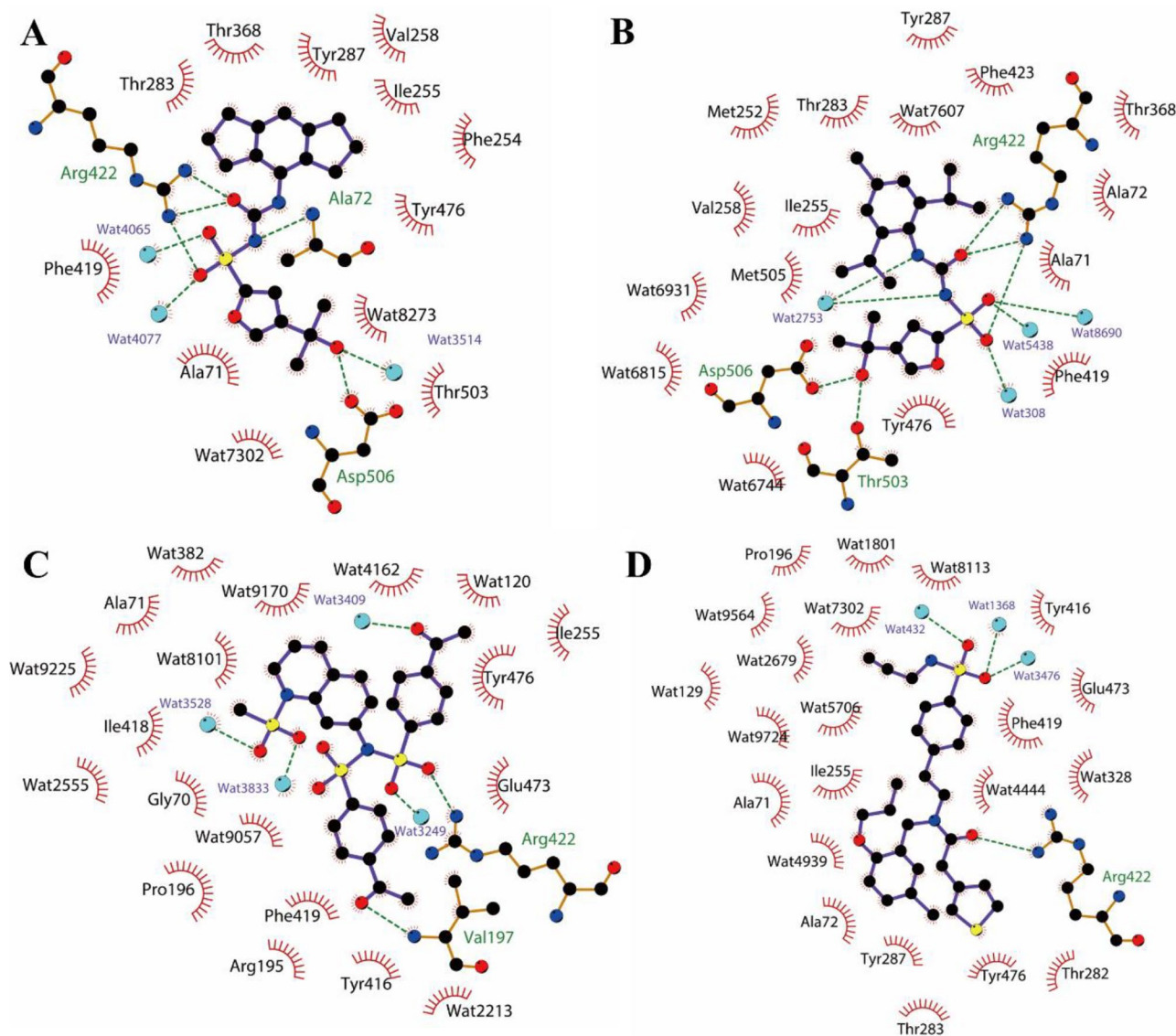


Fig. 3 Residues and water that form hydrophobic and hydrogen bond with the inhibitor at the binding site predicted by the LigPlus. **(A)** NLRP3/MCC950 complex; **(B)** NLRP3/NP3-146 complex; **(C)** NLRP3/(3) complex; **(D)** NLRP3/YQ128 complex

decomposed this energy into contributions from individual residues. This approach allows us to assess the importance of each residue in mediating the interaction between NLRP3 and the inhibitors based on the energy contribution of a single residue. In Fig. 4, we present the residues whose absolute energy contribution to the binding of the four inhibitors exceeds 0.5 kcal/mol. The energy decomposition profiles for the NLRP3/MCC950 and NLRP3/NP3-146 complexes exhibit similarities,

suggesting that MCC950 and NP3-146 bind to NLRP3 in comparable modes. Key residues involved in the interactions of MCC950 and NP3-146 with NLRP3 include Ala71, Ala72, Arg195, Ile255, Val258, Thr283, Thr368, Ile418, Phe419, Arg422, Gln468, Leu472, Glu473, Met505, and Asp506. Notably, the energy contributions of Glu473 and Asp506 are positive, indicating that these residues contribute unfavorably to the binding of MCC950 and NP3-146 to NLRP3. Among these,

Table 2 Summary of hydrogen bond between the ligand and protein

Acceptor	DonorH	Donor	Frac(%) ^a	AvgDist(Å) ^b	AvgAng ^c
MCC950/NLRP3					
ligand@O1	Arg422@HH12	Arg422@NH1	0.7566	2.8111	156.1834
ligand@N2	Ala72@H	Ala72@N	0.3929	2.9182	160.7263
ligand@O1	Arg422@HH22	Arg422@NH2	0.3589	2.8669	147.9582
Asp506@OD1	ligand@H20	ligand@O5	0.3465	2.7100	162.3274
Asp506@OD2	ligand@H20	ligand@O5	0.2973	2.6950	163.1709
Ala72@O	ligand@H14	ligand@N1	0.2537	2.9066	156.1062
NP3-146/NLRP3					
ligand@O5	Arg422@HH12	Arg422@NH1	0.6231	2.8384	154.8306
ligand@O4	Arg422@HH22	Arg422@NH2	0.2572	2.8422	147.2764
ligand@O5	Arg422@HH22	Arg422@NH2	0.1568	2.8922	145.4655
Asp506@OD1	ligand@H3	ligand@O2	0.3608	2.6959	162.1998
Asp506@OD2	ligand@H3	ligand@O2	0.2363	2.6770	163.1343
(3)/NLRP3					
ligand@O8	Val197@H	Val197@N	0.5078	2.8758	158.7179
ligand@O3	Arg422@HH12	Arg422@NH1	0.1053	2.8535	151.8998
ligand@O6	Arg422@HH12	Arg422@NH1	0.0453	2.8396	153.6773
ligand@O3	Arg422@HH22	Arg422@NH2	0.0261	2.8703	151.9890
YQ128/NLRP3					
ligand@O1	Arg422@HH11	Arg422@NH1	0.7720	2.8260	154.3325

^athe frequency of the hydrogen bond in 20,000 conformations is counted

^band ^cDistance and angle of hydrogen bond

Arg422 contributes the most significantly to the binding of both inhibitors. In the compound (3)/NLRP3 complex, the residues Arg195 and Asp506 exhibit positive energy contributions, which are unfavorable for the binding of compound (3) to NLRP3. Similarly, in the YQ-128/NLRP3 complex, the residues Lys76, Arg195, Glu473, and Asp506 contribute positively, indicating an unfavorable interaction between YQ-128 and NLRP3. Furthermore, Fig. 2 reveals that the binding mode of YQ-128 with NLRP3 differs markedly from that of other three compounds, which aligns with our initial analysis of the binding modes of the four inhibitors with NLRP3.

Common features shared by NLRP3-inhibitors recognition

The pharmacophore models for the interactions between the four inhibitors and NLRP3 were generated using the Pymol plug-in AncPhore, as illustrated in Fig. 5. For MCC950 (Fig. 5A), the dominant interaction is hydrophobic, involving the residues Met252, Ile255, Val258 and Tyr287. Additionally, the oxygen and hydrogen atoms in the side chain of residue Ala72 form hydrogen bonds with MCC950, acting as donors and acceptors

respectively. The nitrogen atom in the side chain of residue Arg422 also forms a hydrogen bond with MCC950 as a donor, while the side chain of residue Asp506 forms a hydrogen bond with MCC950 as an acceptor. Due to structural differences, the pharmacophore model for NP3-146 and NLRP3 deviates significantly from that of MCC950. Specifically, NP3-146 exhibits hydrophobic interactions with residues Met252, Ile255, Thr283, and Thr368. Furthermore, residues Arg422 and Asp506 form hydrogen bonds with NP3-146, acting as hydrogen bond receptors and donors, respectively. The pharmacophore models for compound (3) and YQ-128 with NLRP3 primarily involve hydrophobic interactions. For instance, compound (3) interacts hydrophobically with residues Pro196, Val197, and Tyr476, and the residue Pro196 also forms a hydrogen bond with compound (3) as a receptor. Similarly, YQ-128 interacts hydrophobically with residues Ala71, Ala72, Glu473, and Ile255. The findings obtained from the pharmacophore model analysis are in agreement with the previous binding mode analysis, providing further validation of the interaction modes between the inhibitors and NLRP3.

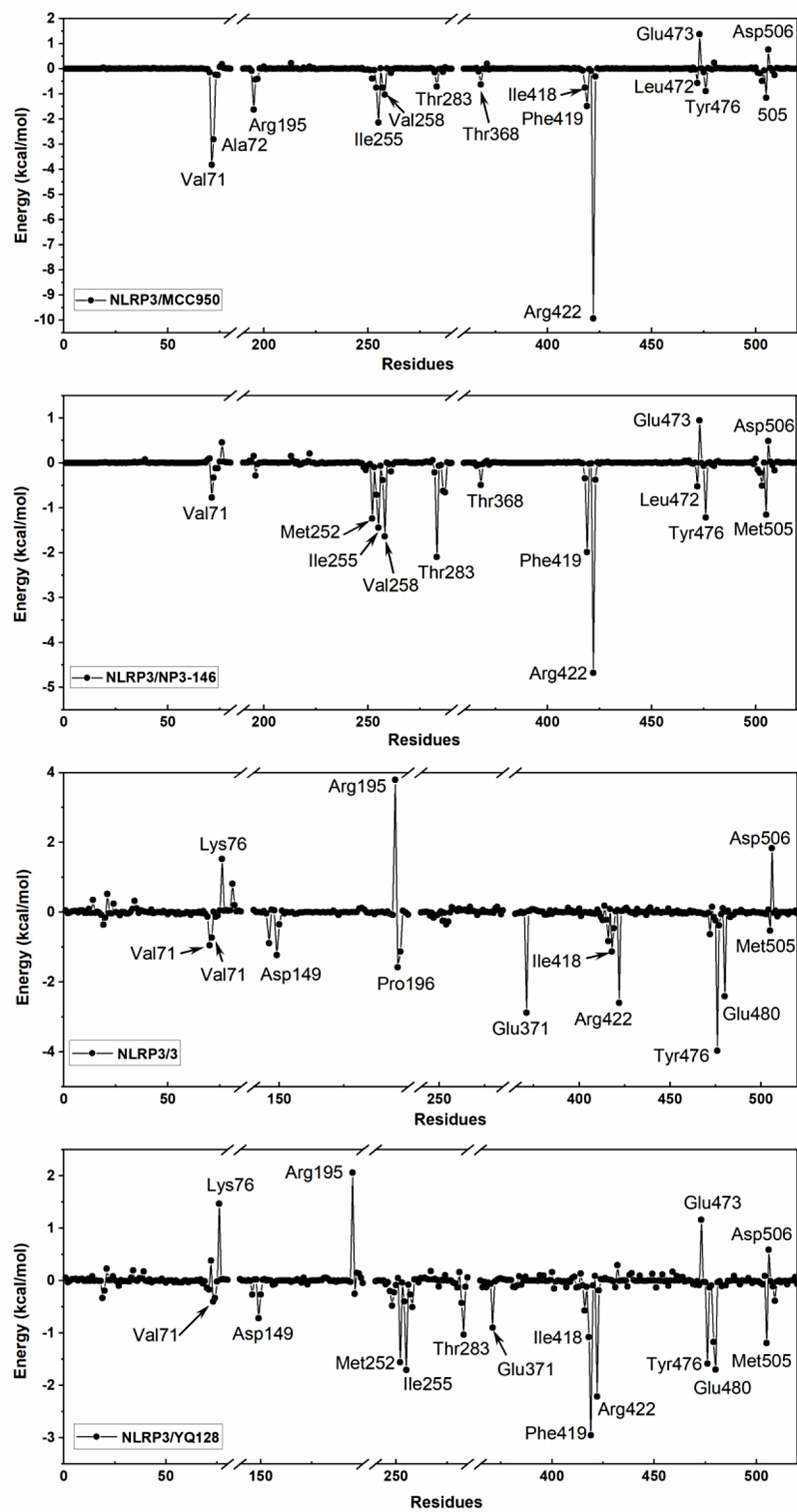


Fig. 4 Per-residue interaction decomposition of the binding free energies for (A) NLRP3/MCC950, (B) NLRP3/NP3-146, (C) NLRP3/(3) and (D) NLRP3/YQ128 complexes

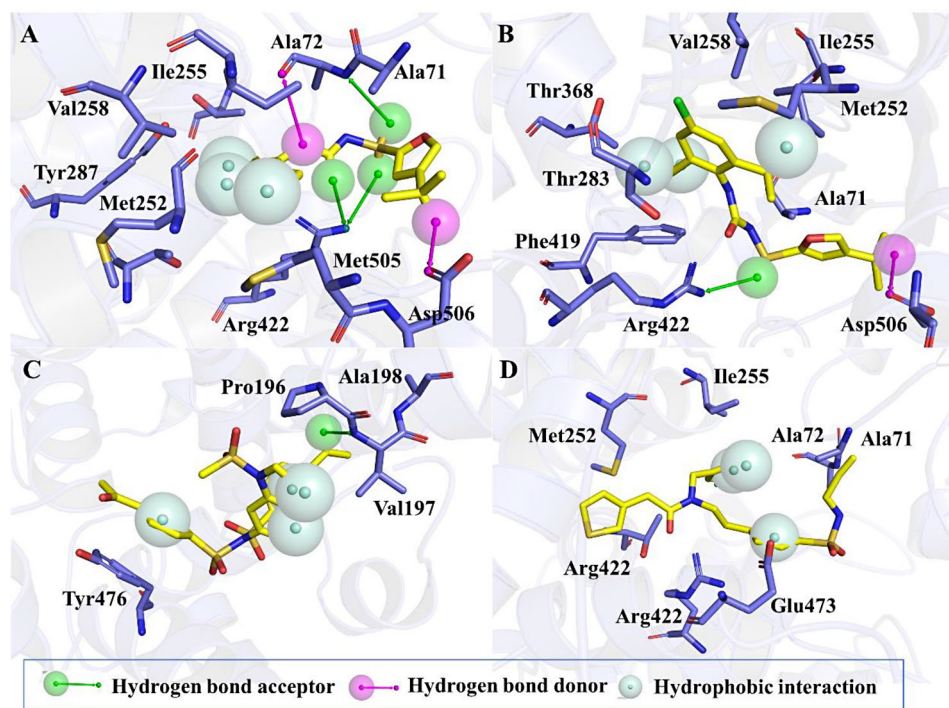


Fig. 5 The pharmacophore model generated by the protocol AncPhore in Pymol. The purple sticks represent the key residues in the pocket of NLRP3, and the purple sticks represents the studied inhibitors MCC950 (in figure **A**), NP3-146 (in figure **B**), (3) (in figure **C**) and YQ-128 (in figure **D**)

Conclusion

In this study, we employed a comprehensive computational approach to elucidate the binding modes of NLRP3 with its representative inhibitors. The total binding free energy of MCC950, as predicted by the MM/GBSA method, was found to be lower than that of the other three inhibitors. This finding is in accordance with experimental observations, which indicate that MCC950 exhibits higher binding affinity compared to the other inhibitors. A detailed decomposition of the residue binding free energies revealed that specific residues located within the binding pocket, namely Ala71, Ala72, Arg195, Ile255, Val258, Thr283, Thr368, Ile418, Phe419, Arg422, Gln468, Leu472, Glu473, Met505, and Asp506, play a crucial role in determining the high bioactivity of NLRP3 inhibitors. By examining the conformations extracted from the equilibrium MD trajectories, we were able to identify key pharmacophore features of the inhibitors that interact with NLRP3. Notably, the primary interaction between the inhibitors and NLRP3 is hydrophobic, and the hydrogen bond formed between the residue Arg422 and the inhibitors is vital for enhancing the activity of the ligands. Our simulation results provide valuable insights into the mechanism of action of NLRP3 inhibitors and their interaction with NLRP3. These findings will undoubtedly facilitate the future development of highly selective inhibitors for NLRP3.

Abbreviations

NLRP3	Nucleotide-binding oligomerization domain, LRR and pyrin domain-containing protein 3
NLRC4	NLR family, CARD domain containing 4
IPAF	Interstitial Pneumonia with Autoimmune Features
AIM2	Absent In Melanoma 2
MM/GBSA	Molecular mechanics/generalized Born surface area
NASH	Nonalcoholic steatohepatitis
NACHT	Nucleotide binding oligomerization domain
CAPS	Cryopyrin-associated periodic syndrome
MD	Molecular dynamics
FEP	Free energy perturbation
TI	Thermodynamic integral
IFD	Induced Fit Docking
PME	Particle Mesh Ewald

Supplementary Information

The online version contains supplementary material available at <https://doi.org/10.1186/s40360-025-00851-0>.

Supplementary Material 1

Acknowledgements

We would like to thank the Guangdong Laboratory of Advanced Energy Science and Technology and the Chinese Academy of Sciences for their computing equipment and software support.

Author contributions

Pingyang Qin and Jizheng Duan: analysis of data, investigation, conceptualization, writing original draft; Yuzhen Niu: methodology, calculation, conceptualization, investigation, resources, review, and editing. Ping Lin: resources, review, and editing.

Funding

This work was supported by the Natural Foundation of Shandong Province (Grant No. ZR2022MB134) and the project of Weifang University of Science and Technology (Grant No. 2024XJKJ06).

Data availability

Data Availability Initial X-ray structures are available at the Protein Data Bank (<https://www.rcsb.org/>).

Declarations

Ethics approval and consent to participate

Not applicable.

Consent for publication

Pingyang Qin, Yuzhen Niu, Jizheng Duan and Ping Lin, hereby grant our explicit consent for the publication in *BMC Pharmacology and Toxicology*.

Competing interests

The authors declare no competing interests.

Received: 18 October 2024 / Accepted: 21 January 2025

Published online: 03 March 2025

References

- Li X, Shang X, Sun L. Tacrolimus reduces atherosclerotic plaque formation in ApoE(-/-) mice by inhibiting NLRP3 inflammatory corpuscles. *Experimental Therapeutic Med.* 2020;19:1393–9.
- Li L, Tang W, Yi F. Role of Inflammasome in chronic kidney disease. *Adv Exp Med Biol.* 2019;1165:407–21.
- Lin L, Xu L, Lv W, Han L, Xiang Y, Fu L, Jin M, Zhou R, Chen H, Zhang A. An NLRP3 inflammasome-triggered cytokine storm contributes to streptococcal toxic shock-like syndrome (STSLs). *PLoS Pathog.* 2019;15:e1007795.
- Li Z, Chen Y, Jiang X, Lu P, Wang C, Li Z, Yu X, Yang Z, Ma S, Du S, et al. Novel sulfonyleurea-based NLRP3 inflammasome inhibitor for efficient treatment of nonalcoholic steatohepatitis, endotoxemic shock, and colitis. *J Med Chem* 2023.
- Shi C, Zhang X, Chi X, Zhou YR, Lyu W, Gao T, Zhou J, Chen Y, Yi C, Sun X, et al. Discovery of NLRP3 inhibitors using machine learning: identification of a hit compound to treat NLRP3 activation-driven diseases. *Eur J Med Chem.* 2023;260:115784.
- Zheng X, Zhao D, Jin Y, Liu Y, Liu D. Role of the NLRP3 inflammasome in gynecological disease. *Biomed Pharmacother.* 2023;166:115393.
- Yang L, Huang Y, Chen F, Wang Y, Su K, Zhao M, Tao W, Liu W. Berberine attenuates depression-like behavior by modulating the hippocampal NLRP3 ubiquitination signaling pathway through Trim65. *Int Immunopharmacol.* 2023;123:110808.
- Coll RC, Hill JR, Day CJ, Zamoshnikova A, Boucher D, Massey NL, Chitty JL, Fraser JA, Jennings MP, Robertson AAB, Schroder K. MCC950 directly targets the NLRP3 ATP-hydrolysis motif for inflammasome inhibition. *Nat Chem Biol.* 2019;15:556–9.
- Coll RC, Robertson AA, Chae JJ, Higgins SC, Muñoz-Planillo R, Insera MC, Vetter I, Dungan LS, Monks BG, Stutz A, et al. A small-molecule inhibitor of the NLRP3 inflammasome for the treatment of inflammatory diseases. *Nat Med.* 2015;21:248–55.
- Tapia-Abellán A, Angosto-Bazarra D, Martínez-Banaclocha H, de Torre-Minguela C, Cerón-Carrasco JP, Pérez-Sánchez H, Arostegui JI, Pelegrin P. MCC950 closes the active conformation of NLRP3 to an inactive state. *Nat Chem Biol.* 2019;15:560–4.
- Dekker C, Mattes H, Wright M, Boettcher A, Hinniger A, Hughes N, Kapps-Fouthier S, Eder J, Erbel P, Stiefel N, et al. Crystal structure of NLRP3 NACHT Domain with an inhibitor defines mechanism of Inflammasome Inhibition. *J Mol Biol.* 2021;433:167309.
- Dai Z, Chen XY, An LY, Li CC, Zhao N, Yang F, You ST, Hou CZ, Li K, Jiang C, et al. Development of Novel Tetrahydroquinoline inhibitors of NLRP3 inflammasome for potential treatment of DSS-Induced mouse colitis. *J Med Chem.* 2021;64:871–89.
- Jiang Y, He L, Green JC, Blevins H, Zhang S. Discovery of second-generation NLRP3 inflammasome inhibitors: Design, synthesis, and biological characterization. *J Med Chem.* 2019:2019.
- Singh R, Purohit R. Computational analysis of protein-ligand interaction by targeting a cell cycle restrainer. *Comput Methods Programs Biomed.* 2023;231:107367.
- Kalsi N, Gopalakrishnan C, Rajendran V, Purohit R. Biophysical aspect of phosphatidylinositol 3-kinase and role of oncogenic mutants (E542K & E545K). *J Biomol Struct Dyn.* 2016;34:2711–21.
- Bhardwaj VK, Purohit R. A comparative study on inclusion complex formation between formononetin and β -cyclodextrin derivatives through multiscale classical and umbrella sampling simulations. *Carbohydr Polym.* 2023;310:120729.
- Bhardwaj V, Singh R, Singh P, Purohit R, Kumar S. Elimination of bitter-off taste of stevioside through structure modification and computational interventions. *J Theor Biol.* 2020;486:110094.
- Singh R, Bhardwaj VK, Sharma J, Das P, Purohit R. Identification of selective cyclin-dependent kinase 2 inhibitor from the library of pyrrolone-fused benzosuberene compounds: an in silico exploration. *J Biomol Struct Dyn.* 2022;40:7693–701.
- Singh R, Bhardwaj VK, Purohit R. Inhibition of nonstructural protein 15 of SARS-CoV-2 by golden spice: a computational insight. *Cell Biochem Funct.* 2022;40:926–34.
- Deng S, Zhang H, Gou R, Luo D, Liu Z, Zhu F, Xue W. Structure-based Discovery of a Novel Allosteric inhibitor against human dopamine transporter. *J Chem Inf Model.* 2023;63:4458–67.
- Tu G, Fu T, Yang F, Yang J, Zhang Z, Yao X, Xue W, Zhu F. Understanding the Polypharmacological profiles of Triple Reuptake inhibitors by Molecular Simulation. *ACS Chem Neurosci.* 2021;12:2013–26.
- Tu G, Xu B, Luo D, Liu J, Liu Z, Chen G, Xue W. Multi-state model-based identification of cryptic Allosteric sites on Human Serotonin Transporter. *ACS Chem Neurosci.* 2023;14:1686–94.
- Xue W, Fu T, Deng S, Yang F, Yang J, Zhu F. Molecular mechanism for the Allosteric inhibition of the human serotonin transporter by Antidepressant Escitalopram. *ACS Chem Neurosci.* 2022;13:340–51.
- Yang F, Yang J, Zhang Z, Tu G, Yao X, Xue W, Zhu F. Recent advances in computer-aided antiviral Drug Design Targeting HIV-1 Integrase and Reverse Transcriptase Associated Ribonuclease H. *Curr Med Chem.* 2022;29:1664–76.
- Guimarães CR, Kopecky DJ, Mihalic J, Shen S, Jeffries S, Thibault ST, Chen X, Walker N, Cardozo M. Thermodynamic analysis of mRNA cap binding by the human initiation factor eIF4E via free energy perturbations. *J Am Chem Soc.* 2009;131:18139–46.
- Gerogiokas G, Calabro G, Henchman RH, Southey MW, Law RJ, Michel J. Prediction of small Molecule Hydration Thermodynamics with Grid Cell Theory. *J Chem Theory Comput.* 2014;10:35–48.
- Hao D, He X, Ji B, Zhang S, Wang J. How well does the Extended Linear Interaction Energy Method Perform in accurate binding Free Energy calculations? *J Chem Inf Model.* 2020;60:6624–33.
- Li P, Niu Y, Li S, Zu X, Xiao M, Yin L, Feng J, He J, Shen Y. Identification of an AXL kinase inhibitor in triple-negative breast cancer by structure-based virtual screening and bioactivity test. *Chem Biol Drug Des.* 2022;99:222–32.
- Niu Y, Ji H. Current developments in extracellular-regulated protein kinase (ERK1/2) inhibitors. *Drug Discov Today.* 2022;27:1464–73.
- Niu Y, Yao X, Ji H. Importance of protein flexibility in ranking ERK2 type I(1/2) inhibitor affinities: a computational study. *RSC Adv.* 2019;9:12441–54.
- Niu Y, Li S, Pan D, Liu H, Yao X. Computational study on the unbinding pathways of B-RAF inhibitors and its implication for the difference of residence time: insight from random acceleration and steered molecular dynamics simulations. *Phys Chem Chem Phys.* 2016;18:5622–9.
- Hsu DJ, Davidson RB, Sedova A, Glaser J. tinyIFD: a high-throughput binding pose refinement Workflow through Induced-Fit ligand docking. *J Chem Inf Model.* 2023;63:3438–47.
- Cieplak P, Cornell WD, Bayly C, Kollman PA. Application of the multimolecule and multiconformational RESP methodology to biopolymers: charge derivation for DNA, RNA, and proteins. *J Comput Chem.* 1995;16:1357–77.
- Bayly CI, Cieplak P, Cornell W, Kollman PA. A well-behaved electrostatic potential based method using charge restraints for deriving atomic charges: the RESP model. *J Phys Chem.* 1993;97:10269–80.
- Fox T, Kollman PA. Application of the RESP Methodology in the parametrization of Organic solvents. *J Phys Chem.* 1998;102:8070–9.
- Tian C, Kasavajhala K, Belfon KAA, Raguette L, Huang H, Miguies AN, Bickel J, Wang Y, Pincay J, Wu Q, Simmerling C. ff19SB: amino-acid-specific protein backbone parameters trained against Quantum Mechanics Energy Surfaces in Solution. *J Chem Theory Comput.* 2020;16:528–52.

37. Jorgensen WL, Chandrasekhar J, Madura JD, Impey RW, Klein ML. Comparison of simple potential functions for simulating liquid water. *J Chem Phys.* 1983;79:926–35.
38. Simmonett AC, Brooks BR. A compression strategy for particle mesh Ewald theory. *J Chem Phys.* 2021;154:054112.
39. Ryckaert J-P, Ciccotti G, Berendsen HJC. Numerical integration of the cartesian equations of motion of a system with constraints: molecular dynamics of n-alkanes. *J Comput Phys.* 1977;23:327–41.
40. Kollman PA, Massova I, Reyes C, Kuhn B, Huo SH, Chong L, Lee M, Lee T, Duan Y, Wang W, et al. Calculating structures and free energies of complex molecules: combining molecular mechanics and continuum models. *Acc Chem Res.* 2000;33:889–97.
41. Lyne PD, Lamb ML, Saeh JC. Accurate prediction of the relative potencies of members of a series of kinase inhibitors using molecular docking and MM-GBSA scoring. *J Med Chem.* 2006;49:4805–8.
42. Yang J, Lin X, Xing N, Zhang Z, Zhang H, Wu H, Xue W. Structure-based Discovery of Novel Nonpeptide inhibitors targeting SARS-CoV-2 M(pro). *J Chem Inf Model.* 2021;61:3917–26.
43. Xue W, Wang P, Li B, Li Y, Xu X, Yang F, Yao X, Chen YZ, Xu F, Zhu F. Identification of the inhibitory mechanism of FDA approved selective serotonin reuptake inhibitors: an insight from molecular dynamics simulation study. *Phys Chem Chem Phys.* 2016;18:3260–71.
44. Lee TV, Johnson RD, Arcus VL, Lott JS. Prediction of the substrate for nonribosomal peptide synthetase (NRPS) adenylation domains by virtual screening. *Proteins-Structure Function Bioinf.* 2015;83:2052–66.
45. Li N, Ainsworth RI, Ding B, Hou T, Wang W. Using hierarchical virtual screening to combat Drug Resistance of the HIV-1 protease. *J Chem Inf Model.* 2015;55:1400–12.
46. Genheden S, Ryde U. The MM/PBSA and MM/GBSA methods to estimate ligand-binding affinities. *Expert Opin Drug Discov.* 2015;10:449–61.
47. Pan D, Xue W, Zhang W, Liu H, Yao X. Understanding the drug resistance mechanism of hepatitis C virus NS3/4A to ITMN-191 due to R155K, A156V, D168A/E mutations: a computational study. *Biochim Et Biophys Acta-General Subj.* 2012;1820:1526–34.
48. Pan D, Niu Y, Xue W, Bai Q, Liu H, Yao X. Computational study on the drug resistance mechanism of hepatitis C virus NS5B RNA-dependent RNA polymerase mutants to BMS-791325 by molecular dynamics simulation and binding free energy calculations. *Chemometr Intell Lab Syst.* 2016;154:185–93.
49. Weiser JR, Shenkin PS, Still WC. Approximate atomic surfaces from linear combinations of pairwise overlaps (LCPO). *J Comput Chem.* 1999;20:217–30.
50. Levitt M, Sander C, Stern PS. Protein normal-mode dynamics - Trypsin-Inhibitor, Crambin, Ribonuclease and lysozyme. *J Mol Biol.* 1985;181:423–47.
51. Dai Q, Yan Y, Ning X, Li G, Yu J, Deng J, Yang L, Li GB. AncPhore: a versatile tool for anchor pharmacophore steered drug discovery with applications in discovery of new inhibitors targeting metallo- β -lactamases and indoleamine/tryptophan 2,3-dioxygenases. *Acta Pharm Sinica B.* 2021;11:1931–46.

Publisher's note

Springer Nature remains neutral with regard to jurisdictional claims in published maps and institutional affiliations.